Pol. J. Environ. Stud. Vol. 34, No. 2 (2025), 1515-1527
DOI: *10.15244/pjoes/187162* ONLINE PUBLICATION DATE: 2024-09-18

Original Research

Agroclimatic Modeling of the Drought Trend in the State of Sinaloa, Mexico, Using the *PDO–AMO* Indices

Omar Llanes Cárdenas[1*], Gabriel E. González González[1], Rosa D. Estrella Gastélum[1], Luz A. García Serrano[2], Román E. Parra Galaviz[3]

[1]Instituto Politécnico Nacional–Centro Interdisciplinario de Investigación para el Desarrollo Integral Regional (CIIDIR-IPN–SINALOA)
[2]Instituto Politécnico Nacional–Centro Interdisciplinario de Investigaciones y Estudios sobre Medio Ambiente y Desarrollo (CIIEMAD-IPN)
[3]Universidad Autónoma de Sinaloa–Facultad de Ingeniería Mochis (UAS–FIM)

Received: 15 January 2023
Accepted: 14 April 2024

Abstract

The goal was to model the trend of meteorological droughts (*MeD*) using the Pacific decadal oscillation (*PDO*) and Atlantic multidecadal oscillation (*AMO*) indices. *PDO–AMO* series were obtained from the National Oceanic and Atmospheric Administration. In 12 weather stations in the state of Sinaloa (1981–2017), the agricultural standardized precipitation index (*aSPI*) and reconnaissance drought index (*RDI*) were calculated. The linear (*SLT*) and non-parametric (*SNT*) significant trends of the *aSPI* and *RDI* were calculated. A principal component analysis was applied to *SLT–SNT* and the first observed principal component ($Z\ PC–1_o$) was extracted. The first calculated principal component was modeled through a linear regression of $Z\ PC–1_c$ (dependent variable) on *PDO–AMO* (independent variables). The correlations between $Z\ PC–1_o$ vs $Z\ PC–1_c = 0.522$ and the linear trend of $Z\ PC–1_c = 0.501$, were significantly different from zero. This study contributes to addressing a research gap not otherwise explored to date in Sinaloa: modeling of the trend in *MeD* through *aSPI–RDI* and *PDO–AMO*. The model can be used to help schedule agricultural irrigation at the most productive times.

Keywords: meteorological drought trend, linear regression, first principal component, predictive model, hypothesis test

Introduction

In recent decades, one of the most damaging agroclimatic phenomena worldwide is the increase in the trend of meteorological droughts (*MeD*) [1-3]. Clarke [4], Spinoni et al. [5], and Syed et al. [6] state that the significant trend of *MeD* can be studied using linear regression (*SLT*) and the non-parametric tests (*SNT*) of Mann–Kendall [3, 7-14]. These *MeD* trends have been applied to the agricultural standardized precipitation index (*aSPI*) [6] and reconnaissance drought index (*RDI*) [9, 10]), mainly due to the fact that they only require effective precipitation (*fP*)

* e-mail: oma_llanes@yahoo.com.mx
Tel./Fax: +(52) 687-872-9625

as input data [15-17] and total precipitation and potential evapotranspiration (*rP–PET*) [16, 18, 19]. Specifically, Syed et al. [6] and Merabti et al. [10] showed that the higher temporal variability of *aSPI* and *RDI* in Saudi Arabia and Algeria respectively can be explained by the first observed principal component ($Z\ PC–1_o$). Additionally, Syed et al. [6] observed that the trend of *aSPI* and *RDI* in Saudi Arabia is highly associated with the variation of the Pacific decadal oscillation (*PDO*). On the other hand, Zhang et al. [20] and Li et al. [21] found in China that the *PDO* and Atlantic multidecadal oscillation (*AMO*) function as predictors of *MeD*. According to Méndez and Magaña [22] and Llanes et al. [23], the *MeD* in northern Mexico can be associated with and predicted through the *–PDO* and *+AMO* phase anomalies since they promote the occurrence of La Niña events (shortage of *rP* and *PET*). The authors of this study have made various contributions in this field of investigation in Sinaloa; for example, Llanes et al. [14] calculated the SNT of *MeD* using the standardized precipitation evapotranspiration index (the trend of *MeD* was not modeled). Llanes et al. [15] found that of four indices of *MeD* that use *fP* (*aSPI* and effective reconnaissance drought index) and *rP* (standardized precipitation index and *RDI*) as explanatory variables, *aSPI* and *RDI* are respectively the indices with the greatest sensitivity to predict rainfed maize yield, which is the crop with the largest sown area in Sinaloa. Finally, Llanes [16] used *PDO–AMO* to predict *aSPI–RDI* (without evaluating the trend).

Therefore, this study is a pioneer for Sinaloa in predicting *SLT–SNT* of *aSPI–RDI* (dependent variables) using *PDO–AMO* (independent variables).

The goal is to model the trend of *MeD* using the *PDO–AMO* indices. This study contributes to the prediction of *MeD* trends in one of the states with the highest agricultural production in Mexico [15]. Understanding these trends can help ensure regional and national food sovereignty, especially in abnormally dry periods [22].

Material and Methods

Generalities

In this study (Sinaloa state) and for the period 1981–2017, the daily data of *rP*, minimum (*minT*) and maximum temperatures (*maxT*) were obtained from Comisión Nacional del Agua–Servicio Meteorológico Nacional (CONAGUA–SMN) [24]. *SLT–SNT* were determined for 12 weather stations after calculation of *aSPI* and *RDI* (using the DrinC program). To obtain the greatest variability of *SLT–SNT*, $Z\ PC–1_o$ was extracted. The monthly series of *PDO* and *AMO* for the period 1981–2017 were obtained from the National Oceanic and Atmospheric Administration (NOAA) [25]. To find the relationship between *SLT–SNT* and *PDO–AMO*, a Pearson correlation (*Pe*) for $Z\ PC–1_o$ vs *PDO–AMO* was applied.

For the calculation of *SLT–SNT* and the correlation of $Z\ PC–1_o$ vs *PDO–AMO*, the following scales and time steps were employed:

1) Nov–Jan, as it is the quarter with the highest sensitivity for predicting rainfed maize yield, considering *aSPI* and *RDI* as independent variables [16].
2) Jun–Nov, since according to Llanes et al. [26], it is the semester where the *rP* with the highest annual contribution occurs.
3) Jul–Sept and Mar–Aug, for being respectively the quarter and semester with the highest annual contribution of *rP* and *PET*. In addition, in these two-time steps, *PDO–AMO* indices have more explanatory power for predicting *aSPI* and *RDI* [16].
4) Oct–Sept was considered as the agricultural year, in addition to being the order of data series in DrinC software, to calculate *aSPI* and *RDI* [27].

After calculating the correlation of $Z\ PC–1_o$ vs *PDO–AMO*, in order to model the first calculated principal component ($Z\ PC–1_c$), a linear regression was applied to $Z\ PC–1_c$ (dependent variable) vs [*Z PDO–6* (Mar–Aug), *Z AMO–3* (Jul–Sep) and *Z AMO–6* (Mar–Aug)] (independent variables) [28]. To validate the predictive sensitivity for the trend of $Z\ PC–1_c$, a *Pe* was applied between $Z\ PC–1_o$ and $Z\ PC–1_c$ for the period 1981–2017. After a standardized normalization [29] and a Shapiro–Wilk normality analysis [27, 28] was done, the trend of $Z\ PC–1_c$ was calculated using linear regression). The correlations $Z\ PC–1_o$ vs $Z\ PC–1_c$ and the linear trend of $Z\ PC–1_c$ were significantly different from zero.

Study Area

This study was carried out in the state of Sinaloa in the northwest of Mexico (Fig. 1). This state is known worldwide for its high volumes of agricultural production (“the breadbasket of Mexico”). For example, it is the national leader in the production of grains, legumes, and vegetables [30]; however, due to its extreme temperature [30] and precipitation gradients [26], the state is vulnerable to the occurrence of intense *PET* and *MeD* [23]. In the data series of this study, the minimum and maximum average values of *rP* and *PET* ranged from *rP* = 439.68 mm (El Playón) to *rP* = 1478.75 mm (Potrerillos) [31] and from *PET* = 1291.17 mm (Potrerillos) to *PET* = 2029.60 mm (Ixpalino). The average aridity index (*A.I.* = 0.54, dry sub-humid) ranged from *A.I.* = 0.25 (semi-arid, El Playón) to *A.I.* = 1.15 (wet, Potrerillos).

Data

For the period 1981–2017, daily data of *rP*, *minT* and *maxT* were obtained from 70 weather stations located in the state of Sinaloa. The data were obtained from the National Water Commission–National Meteorological Service [24] at https://smn.conagua.gob.mx/es/climatologia/informacion-climatologica/informacion-estadistica-climatologica. The proportion of missing data was less than 10% at only twelve stations; therefore, the series from these stations were selected for this study. Missing data were estimated with the multiple imputation method, using the Markov chain Monte Carlo algorithm (MCMC) [32], since according to Aieb et

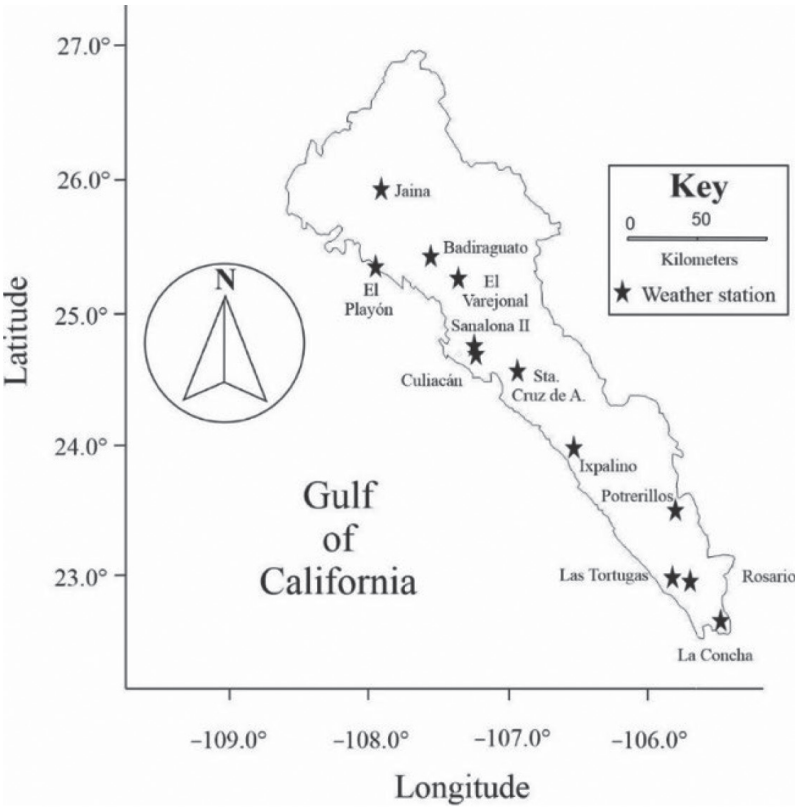

Fig. 1. Study area. Location of weather stations.

al. [33] and Johnson [34], it is the best choice for imputation when the missing data <10%.

Mathematical Equations to Calculate the Indices of Meteorological Drought (MED)

Agricultural Standardized Precipitation Index (aSPI)

The index *aSPI* is a modification of the standardized precipitation index [15, 35, 36]; the difference is that instead of using *rP*, *aSPI* only uses *fP*. In this study, *fP* was calculated with the USDA method–version CROPWAT [37], which, according to Tigkas et al. [15], has been used successfully and on multiple occasions in semi-arid conditions. Equations 1 and 2 characterize *fP*:

$$fP = \frac{rP \cdot (125 - 0.2rP)}{125}; \text{ for } rP \leq 250 \text{ mm} \quad (1)$$

$$fP = (0.1 \cdot rP) + 125; \text{ for } rP > 250 \text{ mm}, \quad (2)$$

where *fP* is the effective precipitation and *rP* is the total precipitation.

To calculate *aSPI*, an index created by Tigkas et al. [15] and applied by Llanes et al. [16] and Javed et al. [38], the following procedure was applied: first, the *fP* series was fitted to the gamma distribution (Equation 3):

$$g(x) = \frac{1}{\beta^{\alpha}\Gamma(\alpha)} x^{\alpha-1} e^{\frac{-x}{\beta}}, \text{ for } x > 0, \quad (3)$$

where the shape and scale parameters are made up of α and β, respectively. $\Gamma(\alpha)$ denotes the gamma function and $x = fp$. Equations 4 and 5 describe the maximum likelihood functions respectively.

$$\alpha = \frac{1}{4A}\left(1 + \sqrt{1 + \frac{4A}{3}}\right) \quad (4)$$

$$\beta = \frac{\bar{x}}{\alpha} \quad (5)$$

where *n* is the number of observations (Equation 6) and where

$$A = \ln(\bar{x}) - \frac{\sum \ln(x)}{n}. \quad (6)$$

To obtain a cumulative probability $G(x)$ from *fP*, Equation 7 was used:

$$G(x) = \frac{\int_0^x t^{\alpha-1} e^{-\frac{t}{\beta}} dt}{\Gamma(\alpha)}. \quad (7)$$

Since *fP* can contain null values, Equation 8 [39] satisfies the cumulative probability:

$$H(x) = q + (1 - q) \cdot G(x). \quad (8)$$

Using Equations 9–11, the cumulative distribution was converted to a normal distribution [40] to obtain the *aSPI* index:

$$aSPI = -\left(t - \frac{c_0 + c_1 t + c_2 t^2}{1 + d_1 t + d_2 t^2 + d_3 t^3}\right), \quad 0 < H(x) \leq 0.5 \quad \text{where } t = \sqrt{\frac{\ln 1}{H(x)^2}} \tag{9}$$

$$aSPI = t - \frac{c_0 + c_1 t + c_2 t^2}{1 + d_1 t + d_2 t^2 + d_3 t^3}, \quad 0.5 < H(x) \leq 1.0 \quad \text{where } t = \sqrt{\frac{\ln 1}{[1 - H(x)^2]}} \tag{10}$$

$$\text{and } c_0 = 2.515517,\ c_1 = 0.802853,\ c_2 = 0.010328,\ d_1 = 1.43278,\ d_2 = 0.189269,\ d_3 = 0.001308. \tag{11}$$

Reconnaissance Drought Index (RDI)

To obtain *RDI*, *rP* and *PET* were first calculated. In this study, *PET* was calculated using the Hargreaves–Samani method [16, 17, 41–46]. Equation 12 defines *PET*:

$$PET = 0.0023 \cdot (mT + 17.8) \cdot (maxT - minT)^{0.5} \cdot Ra, \tag{12}$$

where *PET* is the potential evapotranspiration [mm month^{-1}]; *mT*, *maxT* and *minT* are respectively the average, maximum and minimum temperatures [°C month^{-1}]; and *Ra* is the extraterrestrial solar radiation [mm month^{-1}]. To calculate *RDI*, which was created by Tsakiris [18] and applied by Syed et al. [6] and Vangelis et al. [46], Equations 13 and 14 were used:

$$\alpha_k^{(i)} = \frac{\sum_{j=1}^{k} rP_{ij}}{\sum_{j=1}^{k} PET_{ij}}, i = 1(1) \cdot N, \quad \text{where } j = 1(1) \cdot k \tag{13}$$

$$RDI_n^{(i)} = \frac{a_k^{(i)}}{\overline{a_k^{(i)}}} - 1, \text{ where } \overline{a_k^{(i)}} \text{ is the arithmetic mean of } a_k^{(i)} \tag{14}$$

where (a_k) of *RDI* is calculated for the $i - th$ year on a time basis of k (months), and j is the month of the $i - th$ year. N is the total number of years of the available data.

According to the explanation of Vangelis et al. [46], it was assumed that a_k satisfactorily follows a lognormal distribution. Then, using Equation 15, the standardized *RDI* was calculated:

$$RDI_{st}^{(i)} = \frac{y^{(i)} - \bar{y}}{\hat{\sigma}_y}, \tag{15}$$

where $y^{(i)}$ is $\ln\left(a_k^{(i)}\right)$, $\bar{y}$ is its arithmetic mean and $\hat{\sigma}_y$ is its standard deviation.

Mathematical Equations to Determine Significant Non-Parametric Trends (SNT)

Mann–Kendall Test

Since not all *MeD* data series presented normality, the *SNT* were first calculated. Using Equation 16, the Mann–Kendall test was applied [7, 8].

$$S = \sum_{i=1}^{n-1} \sum_{j=i+1}^{n} sgn(x_j - x_i), \tag{16}$$

where n is the number of data points in the series, x_j and x_i are the data values of items j and i; with the condition $j > i$; and $sgn(x_j - x_i)$ is the sign function. The sign function is described by Equation 17:

$$sgn(x_j - x_i) = \begin{cases} +1, if\ x_j - x_i > 0 \\ 0, if\ x_j - x_i = 0 \\ -1, if\ x_j - x_i < 0. \end{cases} \tag{17}$$

The variance function is defined by Equation 18:

$$Var(S) = \frac{n(n+1)(2n+5) - \sum_{i=1}^{m} t_i(t_i-1)(2t_i+5)}{18}, \tag{18}$$

where n is the number of data points in the series, m is the number of linked groups and t_i is the number of ties in measurement i. Since in this study $n > 10$, the standard normal test Z_s was determined with Equation 19:

$$Z_s = \begin{cases} \frac{S-1}{\sqrt{Var(S)}}, \text{if } S > 0 \\ 0, if\ S = 0 \\ \frac{S+1}{\sqrt{Var(S)}}, \text{if } S < 0. \end{cases} \tag{19}$$

For $Z_s > 0$, it defines an increasing trend and when $Z_s < 0$, a decreasing trend is identified. A *SNT* is defined when $Z_s > |1.96|$ [3].

Sen's Slope Estimate

This statistical test was applied through the following steps: the slope of a trend in the sample from pairs of data was estimated [12] (Equation 20).

$$Q_i = \frac{x_j + x_k}{j - k}, \quad \text{for } i = 1, \ldots, N, \tag{20}$$

where x_j and x_k are the data values at times j and k, with the condition $j > k$. In the event of finding only one datum for each period, Equation 21 was applied:

$$N = \frac{n(n-1)}{2}, \tag{21}$$

where n is the number of periods. If there were multiple observations in one or more time periods, Equation 22 was applied:

$$N < \frac{n(n-1)}{2}, \tag{22}$$

where is the total number of observations. *N* values from Q_i were classified from highest to lowest, and Sen's slope estimator was calculated with the median, Equation 23 was used:

$$Q_{med} = \begin{cases} Q_{\left[\frac{N+1}{2}\right]}, \text{if } N \text{ is odd} \\ Q_{\left[\frac{n}{2}\right]} + Q_{\left[\frac{N+2}{2}\right]}, \text{if } N \text{ is even.} \end{cases} \tag{23}$$

The sign from Q_{med} was the same as that of Z_s (Equation 19) and the magnitude from Q_{med} was the steepness of the trend (Equation 23).

Mathematical Equations to Determine Significant Linear Trends (SLT)

Line Fitting by the Least Squares Method

After calculations of the *SNT*, *SLT* were determined. To calculate *SLT* and based on what was described by Devore [47], it is known that the simplest deterministic relationship between two variables and is the linear relationship, which is expressed by Equation 24:

$$y_i = \beta_0 + \beta_1 x_i. \tag{24}$$

Using Equation 25, the vertical deviation of a point (x_i, y_i) of a line is defined as:

$$y = b_0 + b_1 x. \tag{25}$$

Therefore, the height of the point (x_i, y_i) can be expressed by Equation 26.

$$y_i - (b_0 + b_1 x_i). \tag{26}$$

Then the sum of the squared vertical deviations of the points $(x_1, y_1), \ldots, (x_n, y_n)$, is defined by Equation 27:

$$f(b_0, b_1) = \sum_{i=1}^{n} [y_i - (b_0 + b_1 x_i)]^2, \tag{27}$$

where the estimated points β_0 and β_1, denoted by $\hat{\beta}_0$ and $\hat{\beta}_1$, are called the least squares estimates; that is, they are the values that minimize $f(b_0, b_1)$. $\hat{\beta}_0$ and $\hat{\beta}_1$ are expressed by Equation 28:

$$f(\hat{\beta}_0, \hat{\beta}_1) \leq f(b_0, b_1). \tag{28}$$

Equation 28 can be applied to any value of b_0 and b_1 . Therefore, the estimated regression line (least squares line) is denoted by Equation 29:

$$y = \hat{\beta}_0 + \hat{\beta}_1 x. \tag{29}$$

The minimizing values of and are found by taking the partial derivatives of $f(b_0, b_1)$ with respect to b_0 and b_1 (Eq 28). If the function of a single variable is set equal to zero, the result is Equation 30:

$$f'(b) = 0. \tag{30}$$

Equations 31 and 32 are then solved:

$$\frac{\partial f(b_0, b_1)}{\partial b_0} = \sum_{i=1}^{n} 2(y_i - b_0 - b_1 x_i)(-1) = 0 \tag{31}$$

$$\frac{\partial f(b_0, b_1)}{\partial b_1} = \sum 2(y_i - b_0 - b_1 x_i)(-x_i) = 0. \tag{32}$$

The common factor –2 is canceled and the equations are rearranged, resulting in the system of normal Equations 33 and 34:

$$n b_0 + \left(\sum_{i=1}^{n} x_i\right) b_1 = \sum_{i=1}^{n} y_i \tag{33}$$

$$\left(\sum_{i=1}^{n} x_i\right) b_0 + \left(\sum_{i=1}^{n} x_i^2\right) b_1 = \sum_{i=1}^{n} x_i y_i. \tag{34}$$

These two equations are linear in the two unknowns b_0 and b_1. As long as all the values of x_i are not identical, the least squares estimate is the only solution of the system. The least squares estimate of the slope coefficient b_1 of the true regression line is denoted by Equation 35:

$$b_1 = \hat{\beta}_1 = \frac{\sum_{i=1}^{n}(x_i - \bar{x})(y_i - \bar{y})}{\sum_{i=1}^{n}(x_i - \bar{x})^2} = \frac{S_{xy}}{S_{xx}}. \tag{35}$$

The formulas for calculating the numerator and denominator of $\hat{\beta}_1$ result in Equations 36 and 37:

$$S_{xy} = \sum_{i=1}^{n} x_i y_i - \frac{(\sum_{i=1}^{n} x_i)(\sum_{i=1}^{n} y_i)}{n} \tag{36}$$

$$S_{xx} = \sum_{i=1}^{n} x_i^2 - \frac{(\sum_{i=1}^{n} x_i)^2}{n}. \tag{37}$$

Therefore, the intersection b_0 of the true regression line, which was estimated by least squares, is expressed by Equation 38:

$$b_0 = \hat{\beta}_0 = \frac{\sum y_i - \hat{\beta}_1 \sum x_i}{n} = \bar{y} - \hat{\beta}_1 \bar{x}. \tag{38}$$

To determine *SLT*, in this study the same methodology was used as in Llanes et al. [26], where the sign and magnitude of the slope coefficient $\hat{\beta}_1$ were considered as the phase and magnitude of the *SLT* increase, respectively.

Meteorological Drought (Med) Indices

To calculate meteorological drought, in this study it was decided to choose the indices *aSPI* [16, 27] and *RDI* [16, 27, 44]. *aSPI* and *RDI* require only *fP* [14]) and *rP–PET* [18], respectively, as input data. In addition, these two indices of *MeD* are the most sensitive for semi-arid agricultural regions [16, 38, 48] such as the state of Sinaloa. In this study, the negative anomalies of *aSPI* and *RDI* were considered as dry events, as in Wang et al. [49].

Scales and Time Steps of Meteorological Drought (Med) Indices

To establish the scales and time steps for *MeD*, the associations between *aSPI–RDI* and the following were

calculated: higher predictive sensitivity for rainfed maize yield [3 months (Nov–Jan) [16], semester with the highest annual contribution of *rP* [6 months (Jun–Nov) [26], quarter with the highest annual contribution of *rP* [3 months (Jul–Sep) [17]], semester with the highest annual contribution of *PET* [6 months (Mar–Aug) [17] and due to the follow-up order of agricultural years [16, 27, 50] [12 months (Oct–Sep).

Significant Trends of Meteorological Droughts (Med)

Significant Non-Parametric Trends (SNT)

To identify *SNT* (*MeD* > |*1.96*|), in each series of *aSPI* and *RDI*, the Mann–Kendall method was applied [51, 52]. To estimate the magnitudes of *SNT*, Sen's slope method was applied [10; 51]. The annual results were multiplied by 10 to represent decadal changes.

Significant Linear Trends (SLT)

To reinforce the *SNT* study, a *SLT* analysis was also applied. This tool was based on the least squares method [53]. With the square root of the coefficient of determination (R^2) of each *SLT*, *Pe* was determined [16]. Each was compared with *Cpe* = |0.329|, for *n* = 36 [54]. If *Pe* > |*CPe*|, then .

Climate Indices

Pacific Decadal Oscillation (PDO) and Atlantic Multidecadal Oscillation (AMO)

According to Ormaza et al. [55], PDO is the most important principal component of the monthly sea surface temperature anomalies in the North Pacific (20–65N and 120E–100W). The *AMO* is defined as the average of the sea surface temperature anomalies of the North Atlantic Ocean (0–70 °N) minus the average of the global sea surface temperature [56, 57]. *PDO* and *AMO* monthly data series were obtained from the National Oceanic and Atmospheric Administration [25], at https://psl.noaa.gov/data/climateindices/list/.

Scales and Time Steps of the Pacific Decadal Oscillation (PDO) and Atlantic Multidecadal Oscillation (AMO)

To define the *PDO* and *AMO* indices, the time steps Mar–Aug (6-month) and Jul–Sep (3-month) were used. According to Llanes et al. [17], these two scales and time steps are the ones that register the highest annual accumulated contributions of *PET* and *rP*.

Statistical Pre-Treatment of Data

Prior to the principal component analysis and based on Llanes et al. [16] and Wüthrich and Merz [58], a *Z* standardized normalization was applied to all data series. Using the Shapiro–Wilk methods [59], Anderson–Darling [60], Lilliefors [61], and Jarque–Bera [62], the normality of all series was calculated.

Principal Component Analysis

To extract the most important indices, scales, and time steps, a principal component analysis was applied to all series with *SNT* (*aSPI–3*, Nov–Jan and *aSPI–6*, Jun–Nov) and *SNT* (*aSPI–12*, Oct–Sep; *RDI–6*, Mar–Aug and *RDI–12*, Oct–Sep): $Z\ PC–1_o$ was then extracted [6].

Association and Predictive Model Between the First Principal Component ($Z\ PC–1_o$) vs Pacific Decadal Oscillation (Z PDO) and the Atlantic Multidecadal Oscillation (Z AMO)

To test the association of $Z\ PC–1_o$ vs *Z PDO* and *Z AMO*, a *Pe* correlation analysis was performed [63]. The correlations were $Z\ PC–1_o$ vs *Z PDO–3* (Jul–Sep), *Z PDO–6* (Mar–Aug), *Z AMO–3* (Jul–Sep); and *Z AMO–6* (Mar–Aug) was called $Z\ PC–1_c$. The *Pe* values obtained were compared with *Cpe* = |0.329|, for *n* = 36 [53]. If *Pe* > |*CPe*|, *Pe* was considered significant. To predict $Z\ PC–1_o$, a linear regression was applied, where *Z PDO–3* (Jul–Sep), *Z PDO–6* (Mar–Aug), *Z AMO–3* (Jul–Sep) and *Z AMO–6* (Mar –Aug) were the independent variables.

Validation of Model

A dispersion analysis was carried out between $Z\ PC–1_o$ vs $Z\ PC–1_c$, and a *Pe* correlation was calculated. For the period 1981–2017, and after a Shapiro-Wilk normality analysis, linear regression of $Z\ PC–1_c$ was calculated. The coefficient of *Pe* of the series $Z\ PC–1_c$ was calculated by means of the square root of the coefficient of determination [$Pe = (R^2)^{0.5}$]. A hypothesis test was applied, where the *Pe* coefficients for $Z\ PC–1_o$ vs $Z\ PC–1_c$, as well as for *SLT* of $Z\ PC–1_c$, were compared with *Cpe* = |0.329|, for *n* = 36 [54]. If *Pe* > |*CPe*|, then *Pe* = significantly different from zero. This methodology was developed in accordance with what was described by Llanes et al. [16]. All statistical analyses were carried out with statistical significance = 0.05.

Software Used and Flowchart of the Applied Methodology

For this study, the programs used were DrinC 1.7 (91), XLstat 2023, PAST 4.08, Surfer 10 and CorelDRAW 2019.

In Fig. 2 (flowchart), each step carried out in the methodology of this study can be seen more clearly.

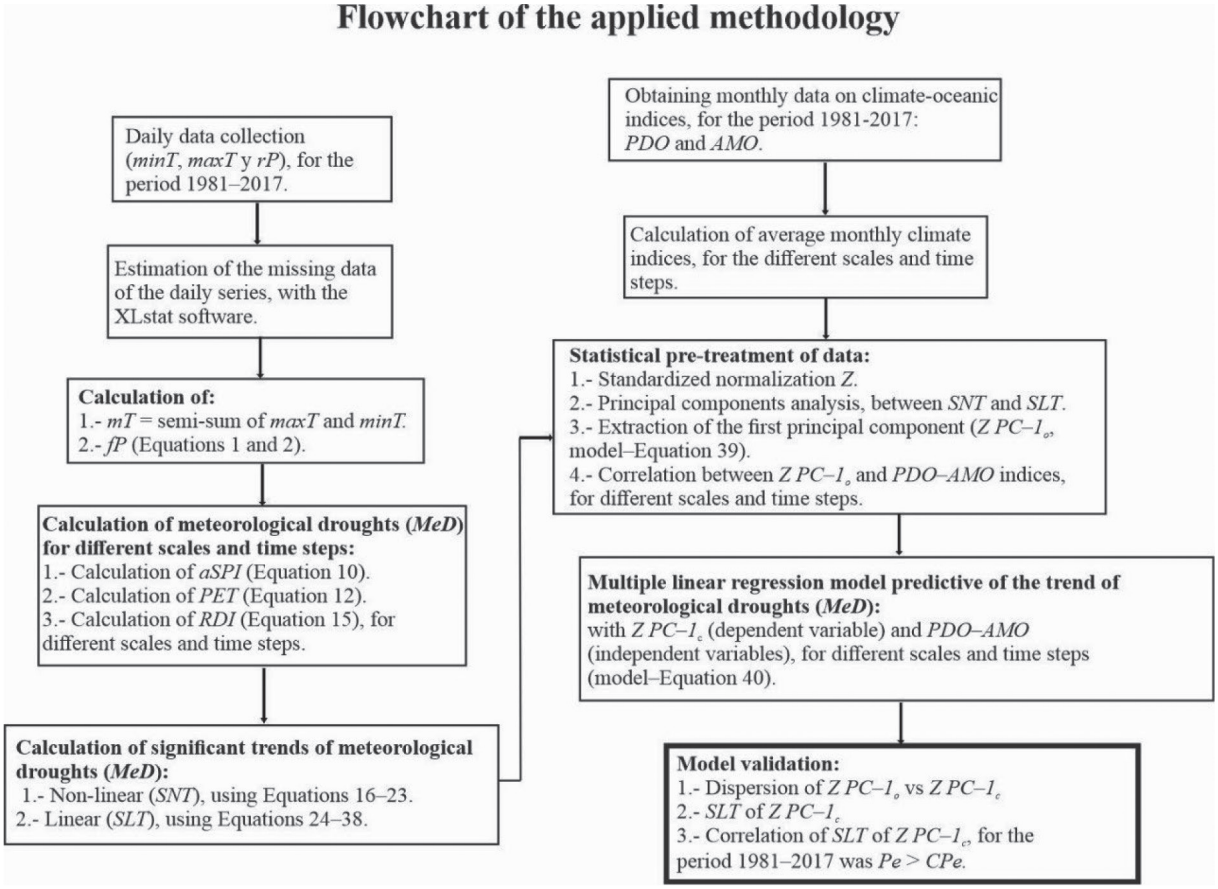

Fig. 2. Flowchart of the methodology applied in this study.

Results and Discussion

Significant Non-Parametric Trends (SNT)

Mann–Kendall Trend Identification

As shown in Table 1, three *SNT* were recorded, one negative [*aSPI–3* (Nov–Jan) = −2.221 for Sanalona II] and two positive [*aSPI–6* (Jun–Nov) = 2.003 for Potrerillos and *RDI–6* (Mar–Aug) = 2.357 for Rosario]. The results from Table 1 can be attributed to the following annual average *rP* trends: a negative trend for Dec–Jan in Culiacán (20 km from Sanalona II) [64], a positive trend for Jun–Sep in Siqueros (17 km from Potrerillos) [64] and minimum accumulated *rP* with greater magnitude for Jan–Dec in Rosario (607.04 mm year^{-1}) [17]. These results are in agreement with Sekhar et al. [65], Llanes et al. [66] and Nandi and Biswas [67], because for $\alpha = 0.05$, significant non-parametric trends must comply with $SNT > |1.96|$.

Table 1. Identification of seasonal and annual significant non-parametric trends (*SNT*, framed magnitudes).

Weather station	*aSPI–3* (Nov–Jan)	*aSPI–6* (Jun–Nov)	*aSPI–12* (Oct–Sep)	*RDI–3* (Jul–Sep)	*RDI–6* (Mar–Aug)	*RDI–12* (Oct–Sep)
Badiraguato	–0.600	0.613	0.191	–0.204	0.899	–0.341
Culiacán	–0.995	1.090	–0.300	1.390	0.095	0.436
El Playón	–0.669	0.490	–0.409	0.913	0.776	0.000
El Varejonal	–0.926	–0.940	0.640	–1.485	1.022	–0.313
Ixpalino	–1.281	–0.668	–0.490	–0.886	–0.354	–1.362
Jaina	–1.648	–0.845	0.259	–0.954	1.308	0.164
La Concha	–1.786	0.736	–0.613	0.804	–0.681	–0.300
Las Tortugas	–0.954	0.518	–0.763	0.586	–0.708	–0.518
Potrerillos	0.885	2.003	1.063	1.090	0.204	1.444
Rosario	–0.765	1.117	0.450	0.409	2.357	1.185
Sanalona II	–2.221	–0.749	–1.498	–0.490	–0.913	–1.731
Sta. Cruz de A.	–0.709	–1.253	0.341	–0.504	1.485	0.654

Magnitude of Significant Non–Parametric Trends (SNT) by Estimating Sen's Slope

In Table 2, the SNT are presented for aSPI–3 (Nov–Jan) = −0.07 year^{-1} and aSPI–6 (Jun–Nov) = 0.05 year^{-1}, for the Sanalona II and Potrerillos stations, respectively. These magnitudes from Table 2 are similar to those calculated by Syed et al. [6], who found an SNT for aSPI = −0.03 yr^{-1} for Saudi Arabia for the period 1985–2020, indicating a continuous increase in dry periods. According to Llanes et al. [16], these same dry periods that occurred in Sinaloa can considerably reduce crop yields, mainly rainfed [68] (such as corn) as well as aquifer recharge, as it is a region with a mostly semi-arid A.I. [69, 70].

Significant Linear Trends (SLT)

In Table 3 and for Sanalona II, the indices *aSPI–3* (Nov–Jan), *aSPI–12* (Oct–Sep) and *RDI–12* (Oct–Sep), registered negative *SLT* (−0.0376, −0.0313 and −0.034, respectively), indicating that in this region (central Sinaloa) the planting–harvest dates of the crops for the autumn–winter and spring–summer cycles should be reassessed, since in future years yields may decrease significantly. *RDI–3* (Jul–Sep) was the only index that did not register *SLT* (Table 3), which can be attributed to the fact that for Jul–Sep, the magnitude of the rainfall irregularity does not seriously affect rainfed crops [71]; that is, the trend of *MeD* is not significant [6; 72].

For Table 4, the most significant *SLT* was found for *aSPI–3* (Nov–Jan) at the Sanalona II station (R^2 = 0.169, r = 0.411), which indicates that for the central region of Sinaloa and for the period Nov –Jan, the greatest negative trends of *MeD* occurred [6; 16].

Normality values (*p–values*) for all data series were Shapiro Wilk (from 0.113 to 0.702), Anderson–Darling (from 0.158 to 0.824), Lilliefors (from 0.071 to 0.859) and Jarque–Bera (from 0.416 to 0.846).

Table 2. Magnitude of seasonal and annual significant non-parametric trends (*SNT*, framed magnitudes).

Weather station	*aSPI–3* (Nov–Jan)	*aSPI–6* (Jun–Nov)	*aSPI–12* (Oct–Sep)	*RDI–3* (Jul–Sep)	*RDI–6* (Mar–Aug)	*RDI–12* (Oct–Sep)
Badiraguato	–0.058	0.078	0.113	–0.052	0.075	–0.106
Culiacán	–0.073	0.060	–0.062	0.059	0.061	0.063
El Playón	–0.063	0.069	–0.034	0.064	0.070	0.043
El Varejonal	–0.061	–0.050	0.044	–0.059	0.042	–0.043
Ixpalino	–0.057	–0.072	–0.088	–0.052	–0.092	–0.082
Jaina	–0.043	–0.054	0.051	–0.032	0.054	0.042
La Concha	–0.070	0.083	–0.124	0.060	–0.069	–0.111
Las Tortugas	–0.044	0.046	–0.098	0.068	–0.071	–0.080
Potrerillos	0.046	0.051	0.072	0.060	0.095	0.089
Rosario	–0.055	0.044	0.058	0.063	0.054	0.056
Sanalona II	–0.065	–0.055	–0.058	–0.054	–0.053	–0.063
Sta. Cruz de A.	–0.058	–0.047	0.079	–0.070	0.091	0.090

Table 3. Phase and magnitude of seasonal and annual significant linear trends (*SLT*, framed magnitudes).

Weather station (Variable *y*)	Drought indices (Variable *x*)					
	aSPI–3 (Nov–Jan)	*aSPI–6* (Jun–Nov)	*aSPI–12* (Oct–Sep)	*RDI–3* (Jul–Sep)	*RDI–6* (Mar–Aug)	*RDI–12* (Oct–Sep)
Badiraguato	*y = –0.010x*	*y = 0.011x*	*y = 0.011x*	*y = –0.004x*	*y = 0.020x*	*y = 0.004x*
Culiacán	*y = –0.024x*	*y = 0.012x*	*y = –0.008x*	*y = 0.020x*	*y = 0.003x*	*y = 0.002x*
El Playón	*y = –0.015x*	*y = 0.008x*	*y = –0.004x*	*y = 0.025x*	*y = 0.012x*	*y = 0.003x*
El Varejonal	*y = –0.016x*	*y = –0.020x*	*y = 0.017x*	*y = –0.026x*	*y = 0.017x*	*y = –0.002x*
Ixpalino	*y = –0.024x*	*y = –0.012x*	*y = –0.009x*	*y = –0.017x*	*y = 0.001x*	*y = –0.014x*
Jaina	*y = –0.025x*	*y = –0.013x*	*y = 0.012x*	*y = –0.014x*	*y = 0.022x*	*y = 0.006x*
La Concha	*y = –0.027x*	*y = 0.011x*	*y = –0.013x*	*y = 0.021x*	*y = –0.008x*	*y = –0.005x*
Las Tortugas	*y = –0.014x*	*y = 0.011x*	*y = –0.018x*	*y = 0.007x*	*y = –0.019x*	*y = –0.016x*
Potrerillos	*y = 0.013x*	*y = 0.036x*	*y = 0.022x*	*y = 0.027x*	*y = 0.007x*	*y = 0.024x*
Rosario	*y = –0.013x*	*y = 0.011x*	*y = 0.009x*	*y = 0.017x*	*y = 0.033x*	*y = 0.022x*
Sanalona II	*y = –0.038x*	*y = –0.014x*	*y = –0.031x*	*y = –0.017x*	*y = –0.007x*	*y = –0.034x*
Sta. Cruz de A.	*y = –0.015x*	*y = –0.018x*	*y = 0.006x*	*y = –0.012x*	*y = 0.014x*	*y = 0.006x*

Table 4. Coefficients of determination and correlation of seasonal and annual significant linear trends (*SLT*, framed magnitudes).

Drought index	Badiraguato	Culiacán	El Playón	El Varejonal	Ixpalino	Jaina	La Concha	Las Tortugas	Potrerillos	Rosario	Sanalona II	Sta. Cruz de A.
aSPI–3 (Nov–Ene)	$R^2 = 0.008$	$R^2 = 0.068$	$R^2 = 0.031$	$R^2 = 0.032$	$R^2 = 0.069$	$R^2 = 0.074$	$R^2 = 0.095$	$R^2 = 0.026$	$R^2 = 0.019$	$R^2 = 0.026$	$R^2 = 0.169$	$R^2 = 0.023$
	$r = 0.089$	$r = 0.261$	$r = 0.176$	$r = 0.179$	$r = 0.263$	$r = 0.272$	$r = 0.308$	$r = 0.161$	$r = 0.138$	$r = 0.161$	$r = 0.411$	$r = 0.152$
aSPI–6 (Jun–Nov)	$R^2 = 0.014$	$R^2 = 0.017$	$R^2 = 0.007$	$R^2 = 0.042$	$R^2 = 0.016$	$R^2 = 0.018$	$R^2 = 0.013$	$R^2 = 0.014$	$R^2 = 0.138$	$R^2 = 0.015$	$R^2 = 0.021$	$R^2 = 0.037$
	$r = 0.118$	$r = 0.130$	$r = 0.084$	$r = 0.205$	$r = 0.126$	$r = 0.134$	$r = 0.114$	$r = 0.118$	$r = 0.371$	$r = 0.122$	$r = 0.145$	$r = 0.192$
aSPI–12 (Oct–Sep)	$R^2 = 0.013$	$R^2 = 0.007$	$R^2 = 0.002$	$R^2 = 0.033$	$R^2 = 0.009$	$R^2 = 0.017$	$R^2 = 0.019$	$R^2 = 0.034$	$R^2 = 0.052$	$R^2 = 0.009$	$R^2 = 0.110$	$R^2 = 0.003$
	$r = 0.114$	$r = 0.084$	$r = 0.045$	$r = 0.182$	$r = 0.095$	$r = 0.130$	$r = 0.138$	$r = 0.184$	$r = 0.228$	$r = 0.095$	$r = 0.332$	$r = 0.055$
RDI–3 (Jul–Sep)	$R^2 = 0.002$	$R^2 = 0.043$	$R^2 = 0.068$	$R^2 = 0.074$	$R^2 = 0.032$	$R^2 = 0.021$	$R^2 = 0.045$	$R^2 = 0.005$	$R^2 = 0.079$	$R^2 = 0.030$	$R^2 = 0.031$	$R^2 = 0.015$
	$r = 0.045$	$r = 0.207$	$r = 0.261$	$r = 0.272$	$r = 0.179$	$r = 0.145$	$r = 0.212$	$r = 0.071$	$r = 0.281$	$r = 0.173$	$r = 0.176$	$r = 0.122$
RDI–6 (Mar–Ago)	$R^2 = 0.041$	$R^2 = 0.001$	$R^2 = 0.015$	$R^2 = 0.031$	$R^2 = 0.001$	$R^2 = 0.053$	$R^2 = 0.006$	$R^2 = 0.038$	$R^2 = 0.006$	$R^2 = 0.118$	$R^2 = 0.005$	$R^2 = 0.022$
	$r = 0.202$	$r = 0.032$	$r = 0.122$	$r = 0.176$	$r = 0.032$	$r = 0.230$	$r = 0.077$	$r = 0.195$	$r = 0.077$	$r = 0.344$	$r = 0.071$	$r = 0.148$
RDI–12 (Oct–Sep)	$R^2 = 0.002$	$R^2 = 0.001$	$R^2 = 0.001$	$R^2 = 0.001$	$R^2 = 0.020$	$R^2 = 0.004$	$R^2 = 0.002$	$R^2 = 0.027$	$R^2 = 0.063$	$R^2 = 0.054$	$R^2 = 0.125$	$R^2 = 0.004$
	$r = 0.045$	$r = 0.032$	$r = 0.032$	$r = 0.032$	$r = 0.141$	$r = 0.063$	$r = 0.045$	$r = 0.164$	$r = 0.251$	$r = 0.232$	$r = 0.354$	$r = 0.251$
	$n = 36$	*CPe* =|0.329|										

Principal Component Analysis

PC–1$_o$ (Equation 39) explained 47.99% of the variance of the drought trend. At the Sanalona II station, the indices with the greatest contribution to *PC–1$_o$* (Equation 20) are presented. In descending order, they are *Z aSPI–12* (Oct–Sep), *Z RDI–12* (Oct–Sep) and *Z aSPI–3* (Nov–Jan). The results from Equation 39 are in agreement with Llanes et al. [66], who calculated a *SNT* in the annual average *rP* for the Sanalona II station in the period 1982–2014.

$$PC\text{–}1_o = 0.26 \cdot [Z\ aSPI - 3\ (\text{Jul–Sep, Sanalona II})] + 0.02 \cdot [Z\ aSPI - 6\ (\text{Jun–Nov, Potrerillos})] + 0.37 \cdot [Z\ aSPI - 12\ (\text{Oct–Sep, Sanalona II})] + 0.02 \cdot [Z\ RDI\text{–}6\ (\text{Mar–Aug, Rosario})] + 0.33 \cdot Z\ RDI - 12\ (\text{Oct–Sep, Sanalona II})]. \quad (39)$$

Association Between Z PC–1$_o$ vs Z Pacific Decadal Oscillation (PDO) and Z Atlantic Multidecadal Oscillation (AMO)

All variables [*Z PC–1$_o$* vs *Z PDO–3* (Jul–Sep), *Z PDO–6* (Mar–Aug), *Z AMO–3* (Jul–Sep) and *Z AMO–6* (Mar–Aug)] presented normality, with Shapiro Wilk values (*W*) ranging from $W = 0.951$ to $W = 0.979$. In general, there were stronger associations between *Z PC–1$_o$* vs *Z PDO* than with respect to *Z AMO*. The highest correlation was obtained for *Z PC–1$_o$* vs *Z PDO–3* (Jul–Sep) = 0.390 (Table 5).

Table 5. Significant coefficients of Pearson correlation (*Pe*) (framed magnitudes) between *Z PC–1$_o$* vs *Z PDO* and *Z AMO*.

Climate index	Coefficients of correlation (*Pe*)
Z PDO–6 (Mar–Aug)	**0.370**
Z PDO–3 (Jul–Sep)	**0.390**
Z AMO–6 (Mar–Aug)	**–0.378**
Z AMO–3 (Jul–Sep)	–0.318
$n = 36$; *CPe* = |0.329|; bold = significant coefficient	

According to Table 5 the *–Z PC–1$_o$* phase trend in Sinaloa is more influenced by *–PDO* phase anomalies (La Niña events) [23], than by *+AMO* phase anomalies (La Niña events) [17]. The time step Jul–Sep (period with the highest accumulated *rP*) is associated more with *–Z PC–1$_o$* phase anomalies than the time step Mar–Aug (period with the highest *PET* accumulated) [17].

These results are in agreement with Huang et al. [72] since these authors point out that *+PDO* anomalies (El Niño events) are highly related to the occurrence of intense hurricanes (absence of meteorological droughts) in the eastern Pacific Ocean (west of Sinaloa), which occur mainly in summer (Jul–Sep).

Model for the First Predicted Principal Component (Z PC–1$_c$)

Following Table 5, the linear regression model for the calculation of *Z PC–1$_c$* (Equation 40) is presented, where the explanatory variables are *Z PDO–6* (Mar–Aug), *Z AMO–6* (Mar–Aug) and *Z AMO–3* (Jul–Sep):

$$Z\ PC - 1_c = 0.01 + 0.34 \cdot [Z\ PDO - 6(\text{Mar} - \text{Aug})] - 0.81 \cdot [Z\ AMO - 6(\text{Mar} - \text{Aug})] + 0.50 \cdot [Z\ AMO - 3(\text{Jul} - \text{Sep})]. \quad (40)$$

Testing the normality of the residuals of the model, we have $W = 0.92$, $p = 0.815$ and average = 0.0. The results from testing the normality of the residuals of the model (Equation 40) show that the data meet the normality assumptions for a linear regression [16].

Validation of Model

The correlation coefficient between $Z\ PC–1_o$ vs $Z\ PC–1_c$ is Pe = 0.522, which was greater than CPe = ï0.329ï(Fig. 3a). The data series of $Z\ PC–1_c$ for the period 1981–2017 presented normality (W = 0.969, $p–value$ = 0.394). The SLT of $Z\ PC–1_c$ was significant: R^2 = 0.255 = Pe = 0.505 > CPe (Fig. 3b).

In Fig. 3a and in accordance with Llanes et al. [16] and OCR [54], and based on *PDO–AMO* indices (independent variables), the proposed model ($–Z\ PC–1_c$, Equation 40) is sensitive ($Pe > CPe$, significantly different from zero) to predicting trends of *MeD* (*aSPI–RDI* indices, dependent variables) in the state of Sinaloa.

The periods 1997–1998, 2007–2008, 2009–2012 and 2016–2017 presented $–Z\ PC–1_c$ phase anomalies (Fig. 3b), which, according to Llanes et al. [16] and Llanes [17], are periods where negative anomalies (droughts) were also recorded in the following drought indices, scales and time steps: *–aSPI–3* (Jul–Sep), *–aSPI–6* (Mar–Aug), *–RDI–3* (Jul–Sep), *–RDI–6* (Mar–Aug) and *–aSPI–3* (Nov–Jan) [15].

Conclusions

For the first time for Sinaloa and through linear regression, the *MeD* trend was sensitively modeled (*aSPI–RDI*, dependent variables), using *PDO–AMO* (Mar–Aug and Jul–Sep, independent variables). This study contributes by demonstrating the utility of a methodology that can be applied to any region of the world where limited meteorological data (temperature–precipitation) is available. One of the limitations of this study is that only the trends of the *aSPI* and *RDI* indices are addressed. Therefore, in future research, the use of other dependent variables is recommended; for example, standardized precipitation evapotranspiration index, rainfall deciles and percentiles, aridity anomaly index, crop moisture index, or hydrothermal coefficient, among other indexes of *MeD*. To try to increase the predictive sensitivity of the proposed model, it is also recommended to expand the study with other independent variables; for example, multivariate *ENSO* index, oceanic El Niño index, southern oscillation index, or North Atlantic oscillation, among other independent variables. In the

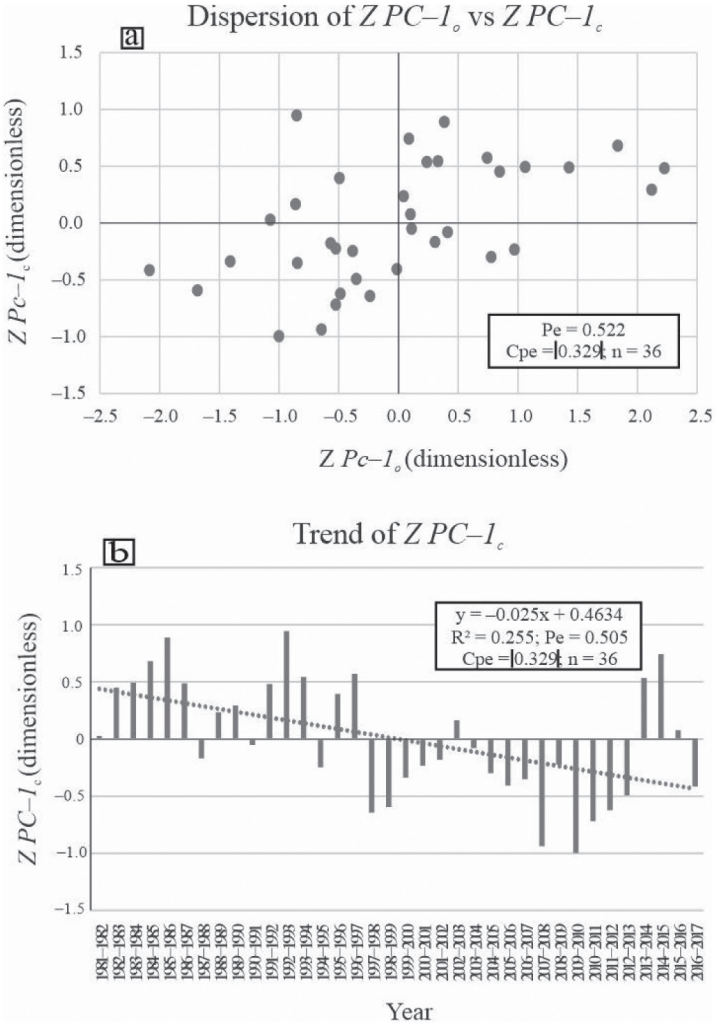

Fig. 3. a) Dispersion between the first principal component observed ($Z\ PC–1_o$) and calculated ($Z\ PC–1_c$) and b) significant linear trend (SLT) of $Z\ PC–1_c$.

validation, two *Pe* were significantly different from zero: 1) *Pe* of *Z PC–1o* vs *Z PC–1$_c$* > *CPe* (Fig. 3a) and 2) *Pe* of *SLT* and for *Z PC–1$_c$* > *CPe* (Fig. 3b). Based on the results obtained, an adjustment is recommended in the sowing dates in Sinaloa, which should avoid the months and the intense anomalies *(> |1.0|)* with phase *+AMO* (Jul–Sep) and *–PDO* (Mar–Aug), because they are generators of intense *MeD*. These results can help to schedule irrigation intelligently in one of the most important agricultural states in North America, called "the breadbasket of Mexico."

Acknowledgments

The authors acknowledge economic support from the Research and Postgraduate Secretariat of the National Polytechnic Institute (SIP-IPN) through the project with registration 20231577.

Conflict of Interest

The authors declare no conflict of interest.

References

1. SERRANO V., DOMÍNGUEZ C.S.M., MURPHY F., HANNAFORD C., REIG J., PEÑA A.F., TRAMBLAY D., TRIGO Y., MAC DONALD R.M., LUNA N. Long-term variability and trends in meteorological droughts in Western Europe (1851–2018). International Journal of Climatology, **41**, E690, **2021**.
2. ALAM J., SAHA P., MITRA R., DAS J. Investigation of spatio-temporal variability of meteorological drought in the Luni River Basin, Rajasthan, India. Arabian Journal of Geosciences, **16** (201), 1, **2023**.
3. GAN R., LI D., CHEN C., YANG F., ZHANG X., GUO X. Spatiotemporal characteristics of extreme hydrometeorological events and its potential influencing factors in the Huaihe River Basin, China. Stochastic Environmental Research and Risk Assessment, **37**, 2693, **2023**.
4. CLARKE R.T. Fitting and testing the significance of linear trends in Gumbel distributed Data. Hydrology nd Earth System Sciences, **6** (1), 17, **2002**.
5. SPINONI J., NAUMANN G., VOGT J., BARBOSA P. European drought climatologies and trends based on a multi-indicator approach. Global and Planetary Change, **127**, 50, **2015**.
6. SYED F.S., ADNAN S., ZAMREEQ A., GHULAM A. Identification of droughts over Saudi Arabia and global Teleconnections. Natural Hazards, **112**, 2717, **2022**.
7. MANN H.B. Nonparametric tests against trend. Econometrica, **13** (3), 245. **1945**.
8. KENDALL M.G. Rank Correlation Methods. Griffin, London. 196 p. **1955**.
9. ABERA T.K., GEBEYEHU A.A. Hydrological and Meteorological Drought Monitoring and Trend Analysis in Abbay River Basin, Ethiopia. Advances in Meteorology, **2022**, 2048077, **2022**.
10. MERABTI A., DAROUICH H., PAREDES P., MEDDI M., PEREIRA L.S. Assessing Spatial Variability and Trends of Droughts in Eastern Algeria Using SPI, RDI, PDSI, and MedPDSI—A Novel Drought Index Using the FAO56 Evapotranspiration Method. Water, **15** (4), 626, **2023**.
11. LIU W., MA S., FENG K., GONG Y., LIANG L., TSUBO M. The Suitability Assessment of Agricultural Drought Monitoring Indices: A Case Study in Inland River Basin. Agronomy, **13** (2), 469, **2023**.
12. SEN P.K. Estimates of the regression coefficient based on Kendall's Tau. Journal of the American Statistical Association, **63** (324), 1379, **1968**.
13. GUO W., HUANG S., ZHAO Y., LENG G., ZHAO X., LI P., NIE M., HUANG Q. Quantifying the effects of nonlinear trends of meteorological factors on drought dynamics. Natural Hazards, **117**, 2505, **2023**.
14. LLANES C.O., PEINADO G.H.J., MONTIEL M.J., NORZAGARAY C.M., GONZÁLEZ O.H.A., CAMPISTA L.S. Seasonal trend indicators and return periods of meteorological drought in the northern States of Mexico. Polish Journal of Environmental Studies, **26** (4), 1471, **2017**.
15. TIGKAS D., VANGELIS H., TSAKIRIS G. Drought characterization based on an agriculture-oriented standardised precipitation index. Theoretical and Applied Climatology, **135**, 1435, **2019**.
16. LLANES C.O., NORZAGARAY C.M., GAXIOLA A., PÉREZ G.E., MONTIEL M.J., TROYO D.E. Sensitivity of Four Indices of Meteorological Drought for Rainfed Maize Yield Prediction in the State of Sinaloa, Mexico. Agriculture, **12** (4), 525, **2022**.
17. LLANES C.O. Predictive association between meteorological drought and climate indices in the state of Sinaloa, northwestern Mexico. Arabian Journal of Geosciences, **16** (79), 1, **2023**.
18. TSAKIRIS G. Meteorological Drought Assessment, Paper Prepared for the Needs of the European Research Program MEDROPLAN; Mediterranean Drought Preparedness and Mitigation Planning: Zaragoza, Spain, **2004**.
19. XUN T.Y., LIN N.J., FENG H.Y. A Review on Drought Index Forecasting and Their Modelling Approaches. Archives of Computational Methods in Engineering, **30**, 1111, **2023**.
20. ZHANG L., WU M., ZHENG J., HAO Z. Role of solar activity and Pacific decadal oscillation in the hydroclimatic patterns of eastern China over the past millennium. Global and Planetary Change, **216**, 103905, **2022a**.
21. LI L., ZHAO L., LI Y. Spatiotemporal Characteristics of Meteorological and Agricultural Droughts in China: Change Patterns and Causes. Agriculture, **13** (2), 265, **2023**.
22. MÉNDEZ J., MAGAÑA R. Regional aspects of prolonged meteorological droughts over Mexico. Journal of Climate, **23**, 1175, **2010**.
23. LLANES C.O., GAXIOLA H.A., ESTRELLA G.R.D., NORZAGARAY C.M., TROYO D.E., PÉREZ G.E., RUIZ G.R., PELLEGRINI C.M. Variability and Factors of Influence of Extreme Wet and Dry Events in Northern Mexico. Atmosphere, **9** (4), 122, **2018**.
24. COMISIÓN NACIONAL DEL AGUA (CONAGUA)–SERVICIO METEOROLÓGICO NACIONAL (SMN). Estaciones meteorológicas. Available online: https://smn.conagua.gob.mx/es/climatologia/informacion-climatologica/informacion-estadistica-climatologica. (accessed on 22 October **2022**).
25. NATIONAL OCEANIC AND ATMOSPHERIC ADMINISTRATION (NOAA) DATABASE CLIMATE

INDICES: monthly atmospheric and ocean time. Available online: https://psl.noaa.gov/data/climateindices/list/. (accessed on 15 June **2022**).
26. LLANES C.O., NORZAGARAY C.M., GAXIOLA A., GONZÁLEZ G.G.E. Regional precipitation teleconnected with PDO-AMO-ENSO in northern Mexico. Theoretical and Applied of Climatology, **140**, 667, **2020**.
27. TIGKAS D., VANGELIS H., PROUTSOS N., TSAKIRIS G. Incorporating aSPI and eRDI in Drought indices Calculator (DrinC) Software for Agricultural Drought Characterisation and Monitoring. Hydrology, **9** (6), 100, **2022**.
28. DOS SANTOS S., BEZERRA C.J.J., TÔRRES R.D., DOS SANTOS S.F.D. Climatology and significant trends in air temperature in Alagoas, Northeast Brazil. Theoretical and Applied Climatology, 151, 1805, 2023.
29. SIDIQI M., KASIVISWANATHAN K.S., SCHEYTT T., DEVARAJ S. Assessment of Meteorological Drought under the Climate Change in the Kabul River Basin, Afghanistan. Atmosphere, **14** (3), 570, **2023**.
30. CONSEJO PARA EL DESARROLLO ECONÓMICO DE SINALOA (CODESIN). Sinaloa en números: agricultura en Sinaloa al 2020. Reporte 29 del 2021, 3p., **2021**. https://sinaloaennumeros.codesin.mx/wp-content/uploads/2021/06/Reporte-29-del-2021-de-Agricultura-en-sinaloa-2020.pdf.
31. MONTAÑO L.Y., SOTO J.M., PÁEZ O.F. Seabed morphodynamics of a coastal lagoon of the Gulf of California. Environmental Fluid Mechanics, **23**, 533, **2023**.
32. AUSTIN C.P., VAN BUUREN S. The effect of high prevalence of missing data on estimation of the coefficients of a logistic regression model when using multiple imputation. BMC Medical Research Methodology, **22** (196), 1, **2022**.
33. AIEB A., MADANI K., SCARPA M., BONACCORSO B., LEFSIH K. A new approach for processing climate missing databases applied to daily rainfall data in Soummam watershed, Algeria. Heliyon, **5** (2), e01247, **2019**.
34. JOHNSON M. Lose Something? Ways to Find Your Missing Data. In Proceedings of the Houston Center for Quality of Care and Utilization Studies Professional Development Series, 17 September. Professional Development Seminar Series, **2003**.
35. MCKEE T.B., DOESKEN N.J., KLEIST J. The Relationship of Drought Frequency and Duration to Time Scales. In Proceedings of the Eighth Conference on Applied Climatology, Anaheim, CA, USA, 17–22 January, 179, **1993**.
36. AMANUEL D.J., ADDISU Y.T., TUJUBA K.T. Spatiotemporal analysis of drought in Oromia regional state of Ethiopia over the period 1989 to 2019. Natural Hazards, **117**, 1569, **2023**.
37. XU H., WU M. A First Estimation of County-Based Green Water Availability and Its Implications for Agriculture and Bioenergy Production in the United States. Water, **10** (2), 148, **2018**.
38. JAVED T., ZHANG J., BHATTARAI N., SHA Z., RASHID S., YUN B., AHMAD S., HENCHIRI M., KAMRAN M. Drought characterization across agricultural regions of China using standardized precipitation and vegetation water supply indices. Journal of Cleaner Production, **313**, 127866, **2021**.
39. EDWARDS C., MCKEE T., DOESKEN N., KLEIST J. Historical Analysis of Drought in the United States, 7th Conference on Climate Variations. 77th AMS Annual Meeting. **1997**.
40. ABRAMOWITZ M., STEGUN I.A. Handbook of Mathematical Functions. Dover Publications, New York, 361 p., **1965**.
41. HARGREAVES G.H., SAMANI Z.A. Reference crop evapotranspiration from temperature. Applied Engineering in Agriculture, **1** (2), 96, **1985**.
42. HARGREAVES G.L., HARGREAVES G.H., RILEY J.P. Irrigation water requirements for Senegal River Basin. Journal of Irrigation and Drainage Engineering, **111** (3), 265e275, **1985**.
43. HARGREAVES G.H., ALLEN R.G. History and evaluation of Hargreaves evapotranspiration equation. Journal of Irrigation and Drainage Engineering, **129** (1), 53e63, **2003**.
44. RASSOUL Z.A., REZA M.M. Evaluation of changes in RDIst index effected by different Potential Evapotranspiration calculation methods. Water Resources Management, **31**, 4981, **2017**.
45. HAMAL K., SHARMA S., KHADKA N., HAILE G.G., JOSHI B.B., XU T., DAWADI B. Assessment of drought impacts on crop yields across Nepal during 1987–2017. Meteorological Applications, **27**, e1950, **2020**.
46. VANGELIS H., TIGKAS D., TSAKIRIS G. The effect of PET method on Reconnaissance Drought Index (RDI) calculation. Journal of Arid Environments, **88**, 130, **2013**.
47. DEVORE J.L. Probability and Statistics for Engineering and the Sciences. Eighth edition, Brooks/Cole, Cengage Learning, 776 p., **2010**.
48. NXUMALO G., BASHIR B., ALSAFADI K., BACHIR H., HARSÁNYI E., ARSHAD S., MOHAMMED S. Meteorological Drought Variability and Its Impact on Wheat Yields across South Africa. International Journal of Environmental Research and Public Health, **19** (24), 16469, **2022**.
49. WANG L., CHEN W., ZHOUC W., HUANG G. Understanding and detecting super-extreme droughts in Southwest China through an integrated approach and index. Quarterly Journal of the Royal Meteorological Society, **142**, 529, **2015**.
50. SECRETARÍA DE MEDIO AMBIENTE Y RECURSOS NATURALES (SEMARNAT). Glosario. **2022**. http://dgeiawf.semarnat.gob.mx:8080/approot/compendio_2019/RECUADROS_INT_GLOS/D2_GLOS_AGRIGAN.htm.
51. KAMRUZZAMAN M., ALMAZROUI M., SALAM M.A., ANARUL H.M.MD., MIZANUR R.MD., DEB L., KUMAR K.P., ASAD U.Z.MD., TOWFIQUL I.A.B.R.MD. Spatiotemporal drought analysis in Bangladesh using the standardized precipitation index (SPI) and standardized precipitation evapotranspiration index (SPEI). Scientific Reports, **12**, 20694, **2022**.
52. REN Y., ZHANG F., ZHAO C., WANG D., LI J., ZHANG J., CHENG Z. Spatiotemporal changes of extreme climate indices and their influence and response factors in a typical cold river basin in Northeast China. Theoretical and Applied Climatology, **152**, 1285, **2023**.
53. ZHANG H.C., WU Q., LI F.Y., LI H. Multitask Learning Based on Least Squares Support Vector Regression for Stock Forecast. Axioms, **11** (6), 292, **2022b**.
54. OXFORD CAMBRIDGE AND RSA (OCR). Formulae and statistical tables (ST1). 1–8: database of critical values. https://www.ocr.org.uk/Images/174103-unit-h869-02-statistical-problem-solving-statistical-tables-st1-.pdf. (accessed on 22 August **2022**).
55. ORMAZA G.F.I., ESPINOZA C.M.E., ROA L.H.M. Did Schwabe cycles 19–24 influence the ENSO events, PDO, and AMO indexes in the Pacific and Atlantic Oceans? Global and Planetary Change, **217**, 103928, **2022**.
56. AZUZ A.I., GONZÁLEZ C.C., CUEVAS C.A. Predicting the Temporal Structure of the Atlantic Multidecadal Oscillation (AMO) for Agriculture Management in

Mexico's Coastal Zone. Journal of Coastal Research, **35** (1), 210, **2019**.
57. CHEN Z., WU R., ZHAO Y., WANG Z. Roles of dynamic and thermodynamic effects in seasonal mean surface air temperature trends over Central Asia during 1979–2018. Climate Dynamics, **60**, 2331, **2023**.
58. WÜTHRICH M.V., MERZ M. Statistical Foundations of Actuarial Learning and its Applications. Springer Actuarial. 605 p., **2023**.
59. HOŁYŃSKA M., SŁUGOCKI Ł. Freshwater microcrustaceans (Copepoda: Cyclopidae) on islands: a review. Hydrobiologia, **850**, 183, **2023**.
60. REY R.D.C., DOMÍNGUEZ I., OVIEDO O.E.R. Effect of agricultural activities on surface water quality from Paramo ecosystems. Environmental Science and Pollution Research, **29**, 83169, **2022**.
61. WEI J. The adoption of repeated measurement of variance analysis and Shapiro–Wilk test. Frontiers of Medicine, **16** (4), 659, **2022**.
62. MANASSEH C.O., IROHA M.N., OKERE I.K., NWAKOBY C.I., OKANYA C.O., NWONYE N., ODIDI O., INYIAMA I.O. Application of Markov chain to share price movement in Nigeria (1985–2019). Future Business Journal, **8** (1), 59, **2022**.
63. RESTREPO B.L.F., GONZÁLEZ L.J. From Pearson to Spearman. Revista Colombiana de Ciencias Pecuarias, **20** (2), 183, **2007**.
64. LLANES C.O., NORZAGARAY C.M., MUÑOZ S.N.P., RUIZ G.R., TROYO D.E., ÁLVAREZ R.P. Hydroclimatic trends in areas with high agricultural productivity in northern Mexico. Polish Journal of Environmental Studies, **24** (3), 1165, **2015**.
65. SEKHAR M.S., PRASAD S.R., MAITY R. Climate change may cause oasification or desertification both: an analysis based on the spatio-temporal change in aridity across India. Theoretical and Applied Climatology, **155**, 1167, **2024**.
66. LLANES C.O., NORZAGARAY C.M., PÉREZ G.E., GAXIOLA A., LÓPEZ R.J.S., GONZÁLEZ G.G.E. Trend analysis and historical and recent return periods of erosivity indicators in the state of Sinaloa, Mexico. Arabian Journal of Geosciences, **13**, 212, **2020**.
67. NANDI S., BISWAS S. Spatiotemporal distribution of groundwater drought using GRACE-based satellite estimates: a case study of lower Gangetic Basin, India. Environmental Monitoring and Assessment, **196**, 151, **2024**.
68. SOUSA L.J.J., RODRIGUES B.F.N., CAVALCANTE P.E., MARIANO I.A.L. Rainfed Crops Forecasting in the Semi-arid Region under Scenarios of Rainfall Instability in Ceará, Brazil. Journal of Agricultural Science and Technology, **A12**, 43, **2022**.
69. ATASHI Y.S.S., MOTAMEDVAZIRI B., ZEYNALABEDIN H.S., AHMADI H. Reciprocal analysis of groundwater potentiality and vulnerability modeling in the Bahabad Plain, Iran. Environmental Science and Pollution Research, **30**, 39586, **2023**.
70. BANDAK S., REZA S.A.M.N., ZEINALI E., BANDAK I. Effects of superabsorbent polymer A200 on soil characteristics and rainfed winter wheat growth (Triticum aestivum L.). Arabian Journal of Geosciences, **14** (712), 1, **2021**.
71. HAQUE M.A., ZHU X., DUNKERLEY D., HENLEY J.B. Observed meteorological drought trends in Bangladesh identified with the Effective Drought Index (EDI). Agricultural Water Management, **255**, 107001, **2021**.
72. HUANG C., LIU H., LI H., ZUO J., WANG R. Combined effects of ENSO and PDO on activity of major hurricanes in the eastern North Pacific. Climate Dynamics, **62**, 1, **2023**.